Chemical Engineering Journal 157 (2010) 121–130

Contents lists available at ScienceDirect

Chemical Engineering Journal

journal homepage: www.elsevier.com/locate/cej

Catalytic hydrodechlorination at low hydrogen partial pressures: Activity and selectivity response

Satyakrishna Jujjuri[a], Mark A. Keane[b,*]

[a] Department of Chemical and Materials Engineering, University of Kentucky, Lexington, KY, USA
[b] Chemical Engineering, School of Engineering and Physical Sciences, Heriot-Watt University, Edinburgh EH14 4AS, Scotland, United Kingdom

ARTICLE INFO

Article history:
Received 17 September 2009
Received in revised form 3 November 2009
Accepted 4 November 2009

Keywords:
Chlorobenzene
1,3-Dichlorobenzene
Pd/silica catalyst
Hydrodechlorination kinetics
Hydrogen partial pressure

ABSTRACT

The gas phase hydrodechlorination (HDC) of chlorobenzene (CB) and 1,3-dichlorobenzene (DCB) (373 K ≤ T ≤ 423 K, P_{total} = 1 atm) was performed over Pd/SiO_2 (1.4–8.3%, w/w Pd) where the hydrogen partial pressure (P_{H_2}) was varied from 0.046 to 0.925 atm. The catalysts have been characterized in terms of BET area, temperature programmed reduction (TPR), hydrogen chemisorption/temperature programmed desorption (TPD) and TEM analyses. The HDC response to changes in contact time, chloroarene feed linear velocity and catalyst particle size were evaluated to establish reaction conditions wherein transport constraints were minimized, *i.e.* contact time = 2.33 s, feed rate = 0.014 mol_{Cl} h^{-1} and particle size = 45–75 μm. HDC selectivity was found to be influenced by transport constraints, which resulted in a preferential partial HDC of 1,3-DCB. Under conditions of chemical control, larger Pd particles (mean values in the range 3–9 nm) delivered higher specific HDC rates. The dependence of HDC rate on P_{H_2} can be accounted for in terms of a Langmuir–Hinshelwood type model involving dissociative adsorption of H_2 and associative adsorption of chloroarene with competition for surface sites. Applicability of this Model is demonstrated in terms of the χ^2 (chi-square) test where the kinetic Models were discriminated on the basis of the standard F-test (% confidence). A dependence of HDC selectivity on P_{H_2} is demonstrated where the conversion of 1,3-DCB at a molar H_2/DCB inlet ≤ 1.25 (P_{H_2} ≤ 0.092 atm) resulted in a higher selectivity to benzene as a result of a lesser competition for surface sites.

1. Introduction

Chlorobenzenes find widespread use in the manufacture of nitrochlorobenzenes, pesticides and dyes, as lubricants, deodorants, degreasing solvents and heat transfer agents [1]. However, chlorobenzenes are well established as persistent toxins for which the environment has little assimilative capacity [2,3]. While global environmental systems are extremely resilient, there is a limit to the pollution burden that can be sustained and an unabated entry of chlorinated compounds into the environment would result in dramatic adverse effects to human health, agricultural productivity and natural ecosystems [4]. Chlorobenzenes, with LC_{50} (lethal concentration, 50%) values spanning the range 2–20 mg dm^{-3}, have been listed for some time by US and European regulatory authorities as "priority pollutants", specifically targeted in terms of emission control [5,6]. Catalytic hydrodechlorination (HDC) is a "green" non-destructive chloro-waste treatment that involves hydrogen cleavage of C–Cl bonds, lowering toxicity and generating reusable raw material. As part of a programme of environmental catalysis, we have examined the action of supported transition metals in promoting gas and liquid phase HDC of chlorobenzenes [7–13]. Taking an overview of the pertinent literature [14–19], Pd emerges as the most efficient metal to promote reductive dehalogenation. In supported metal systems, the nature of the support can impact on the catalytic performance of the metal phase in a number of ways [20]. Halligudi et al. [21], in studying the HDC of 1,2-dichlorobenzene (1,2-DCB) over Pd supported on MgO, SiO_2, activated carbon and γ-Al_2O_3 found that variations in catalytic activity could be linked to the acid/base properties of the carrier. Gampine and Eyman [22], in their examination of DCB HDC over a range of oxide ($TiZrAlO_x$, $TiZrSiO_x$, ZrO_2, Al_2O_3, TiO_2 and SiO_2) supported Pd catalysts, attributed activity/selectivity variations to differences in metal–support interaction and/or adsorption properties of the support. Moreover, we have reported an enhancement of Pd HDC rate (by more than an order of magnitude) through the introduction of lanthanide or alkaline earth promoters and ascribed this response to hydrogen transfer (*via* lanthanide hydride) and electron transfer (*via* the alkaline earth metal) [7–10].

This paper focuses on the feasibility of controlling HDC activity/selectivity over Pd/SiO_2 by varying H_2 partial pressure (from sub-stoichiometric to excess quantities). The HDC studies reported to date have employed H_2 in excess of the stoichiometric require-

* Corresponding author. Tel.: +44 0131 4514719.
E-mail address: M.A.Keane@hw.ac.uk (M.A. Keane).

1385-8947/$ – see front matter © 2009 Elsevier B.V. All rights reserved.
doi:10.1016/j.cej.2009.11.004

Nomenclature

E_a	apparent activation energy (kJ mol^{-1})
$F_{Cl_{in}}$	inlet molar feed rate of organic-Cl (mol$_{Cl}$ h^{-1})
k	pseudo-first order rate constant (mol$_{Cl}$ h^{-1} g$_{Pd}$$^{-1}$)
k_{ClA}	dechlorination rate constant of CB or DCB (mol$_{Cl}$ h^{-1} g$_{Pd}$$^{-1}$)
K_{ClA}	equilibrium constant for associative adsorption of CB or DCB (atm^{-1})
K_H	equilibrium constant for the dissociative adsorption of H_2 (atm^{-1})
K_{H_2}	equilibrium constant for the associative adsorption of H_2 (atm^{-1})
K_{HCl}	equilibrium constant for the displacement of adsorbed HCl by ClA
P_{ClA}	partial pressure of CB or DCB (atm)
P_{H_2}	partial pressure of hydrogen (atm)
P_{HCl}	partial pressure of HCl (atm)
r_{Cl}	specific HDC rate (mol$_{Cl}$ h^{-1} m$_{Pd}$$^{-2}$)
$r_i^{calc}(x_i, y_i)$	calculated reaction rate (mol$_{Cl}$ h^{-1} g$_{Pd}$$^{-1}$)
r_i^{exp}	experimental reaction rate (mol$_{Cl}$ h^{-1} g$_{Pd}$$^{-1}$)
S_{CB}	chlorobenzene selectivity (%)
T	temperature (K)
W	weight of catalyst (g)
X_{Cl}	fractional dechlorination
$X_{CB(DCB)}$	fractional CB (or DCB) consumption
x_i	independent variables in non-linear regression
y_i	fitting parameters to the non-linear model

Greek letters

θ_{ClA}	fraction surface coverage by associatively adsorbed CB or DCB
θ_H	fractional surface coverage by hydrogen atoms
θ_{H_2}	fractional surface coverage by hydrogen molecules
θ_{HCl}	fractional surface coverage by HCl
θ_V	fraction of vacant sites
τ	contact time (s)
χ^2	chi-square test

ment, *e.g.* by a factor of 10 [17], 8 [22] and 3 [23]. In many instances it is not possible to arrive at an inlet H_2/reactant ratio from the information that has been provided. Use of a dilute hydrogen stream is an important consideration in developing an effective (low cost) process where issues of atom efficiency and recycle must be addressed [24,25]. There have only been a few published kinetic studies concerning chlorobenzene(s) HDC over supported Pd [17,26,27], in part due to the high HDC activity and appreciable deactivation, the latter the result of coking [16], poisoning [22,23,28] and sintering [22]. Lopez et al. [17] adopted a standard Langmuir–Hinshelwood approach to model HDC kinetics over Pd/Al_2O_3. Coq et al. [27] and Bodnariuk et al. [26] proposed a surface mechanism to account for HDC kinetics over alumina supported Pd, Rh, Pd–Rh and Pd–Sn where chlorobenzene and HCl compete for Pd–H surface sites to form surface metal chloride species. Kinetic studies of HDC over Ni based catalysts have addressed surface reaction/desorption dynamics [29] and the role of spillover hydrogen in determining HDC rate on a non-uniform surface [30]. We view catalytic HDC as an innovative means of transforming overly chlorinated "waste" into a recyclable product. Taking 1,3-DCB as representative of an unwanted chloro-product, we address issues of sustainability by examining the impact that variations in the inlet H_2 partial pressure have on the HDC performance of Pd/SiO_2.

2. Experimental

2.1. Catalyst preparation, activation and characterization

Pd loaded (1.4–8.3%, w/w Pd) silica (Cab–O–Sil 5 M, BET area = 194 m^2 g^{-1}) catalyst precursors were prepared by standard impregnation with aqueous $Pd(NO_3)_2$ solutions where the solution was added dropwise at 363 K to the substrate with constant agitation (500 rpm). The impregnated samples were dried in a flow of He at 383 K for 3 h and stored under He at room temperature. The metal content (accurate to within ±2%) was measured by inductively coupled plasma-optical emission spectrometry (ICP-OES, Vista-PRO, Varian Inc.) from the diluted extract in HF. The catalyst powder was sieved (ATM fine test sieves) into batches with particle diameters in the range: 150–106 μm (100–140 mesh); 106–75 μm (140–200 mesh); 75–45 μm (200–325 mesh); 45–38 μm (325–400 mesh). The Pd content in each sieved batch was constant within the ICP analysis error. BET surface area, temperature programmed reduction (TPR), H_2 chemisorption and temperature programmed desorption (TPD) were determined using the commercial CHEMBET 3000 (Quantachrome) unit. The total surface area was recorded in a 30% (v/v) N_2/He flow; pure N_2 (99.9%) served as the internal standard. After outgas for 30 min, at least two cycles of N_2 adsorption–desorption in the flow mode were employed using the standard single point BET method. In the TPR analysis, the samples (*ca.* 50 mg) were heated in a U-shaped Pyrex cell (10 cm × 3.76 mm i.d.) in 20 cm^3 min^{-1} (Brooks mass flow controlled) 5% (v/v) H_2/N_2 to 573 K at 10 K min^{-1} and the effluent gas passed through a liquid N_2 trap. Changes to the carrier gas composition were monitored by a thermal conductivity detector (TCD) with data acquisition/manipulation using the TPR Win^{TM} software. The samples were swept with 20 cm^3 min^{-1} dry N_2 for 1 h at 573 K, cooled to room temperature and subjected to H_2 chemisorption using a pulse (50 μl) titration procedure. Any possible contribution due to β-palladium hydride formation can be discounted as the H_2 partial pressure (<2 Torr) was below that (>11 Torr) required to generate the hydride [22]. The sample was thoroughly flushed with pure N_2 (20 cm^3 min^{-1}) for 30 min to remove any weakly bound H_2. Temperature programmed desorption (TPD) was conducted in the N_2 flow at 50 K min^{-1} to 873 K with a final isothermal hold of 15 min. Based on TCD calibrations and analysis of the effluent gas using a MICROMASS PC Residual Gas Analyser, the TPD profiles recorded in this paper can be attributed solely to H_2 release [8]. The BET surface area and H_2 uptake values were reproducible to within ±5% and the values quoted in this paper are the mean. Transmission electron microscopy (TEM) analysis was carried out using a Philips CM20 TEM microscope operated at an accelerating voltage of 200 kV. The passivated (in 1% (v/v) O_2/He) samples were prepared for analysis by ultrasonic dispersion in butan-2-ol, evaporating a drop of the resultant suspension onto a holey carbon support grid. The mean particle sizes presented in this study are based on a measurement of over 650 individual particles; Pd size detection limit was *ca.* 0.1–0.2 nm.

2.2. Catalytic system

Post-TPR, the reactions were conducted *in situ* with a co-current flow of the chloroarene feed in H_2 or H_2/He. The reactor/procedure has been described in some detail elsewhere [11,31] but features pertinent to this study are given below. A layer of glass beads above the catalyst bed ensured that the reactants were vaporized and reached reaction temperature before contacting the catalyst. A Model 100 (kd Scientific) microprocessor controlled infusion pump was used to deliver the aromatic feed, *via* a glass/teflon air-tight syringe and teflon line, at a fixed calibrated flow rate. All the reactions were carried out in the *T*

Table 1
Pd content, BET surface area, molar H/Pd ratio associated with the supported Pd hydride, H_2 uptake and release (during TPD), Pd particle size distribution and mean diameter (d).

	Loading (% w/w)	BET area ($m^2\,g^{-1}$)	H/Pd (TPR) (mol/mol)	H_2 chemisorption ($\mu mol\,g^{-1}$)	H_2 desorbed (TPD) ($\mu mol\,g^{-1}$)	Pd size distribution (nm)	d (nm)
Pd/SiO_2-I	1.4	190	0.20	23	21[a], 742[b]	1–12	3.2
Pd/SiO_2-II	5.4	178	0.30	41	43[a], 753[b]	2–30	6.5
Pd/SiO_2-III	8.3	174	0.31	44	45[a], 701[b]	2–40	9.4

[a] Desorption at $T < 700$ K.
[b] Desorption at 873 K.

range 373–423 K where isothermal operation was ensured by diluting the catalyst bed with ground glass. Chlorobenzene (CB, Aldrich, 99.9%) and 1,3-dichlorobenzene (1,3-DCB, Aldrich, 99%) reactants were used without further purification. HDC performance was evaluated over a range of process conditions: inlet hourly Cl/Pd mol ratio = 3.6×10^3; contact time (τ) = 0.22–2.67 s; P_{H_2} = 0.046–0.925 atm; $W_{catalyst}/F_{Cl}$ = 0.7–3.5 g h mol_{Cl}^{-1}. The effect of varying the linear velocity of the liquid reactant on HDC activity/selectivity was studied where the liquid feed rate was altered from 0.82 $cm^3\,h^{-1}$ (0.19 $\mu m\,s^{-1}$) to 1.44 $cm^3\,h^{-1}$ (0.33 $\mu m\,s^{-1}$) while maintaining a constant (3 h^{-1}) liquid hourly space velocity (LHSV), *i.e.* constant $F_{CB(DCB)}/V_{catalyst}$. Variation in contact time was achieved by adjusting the bed volume but keeping a constant inlet Cl/Pd ratio at a fixed carrier gas linear velocity (0.5 cm s^{-1}) where there were no flow fluctuation and negligible pressure drop across the catalyst bed. In a series of blank tests, passage of each reactant in a stream of H_2 through the empty reactor, *i.e.* in the absence of catalyst, did not result in any detectable conversion. The reactor effluent was frozen in a liquid nitrogen trap for subsequent analysis using a PerkinElmer Auto System XL chromatograph equipped with a split/splitless injector and a flame ionization detector, employing a DB-1 50 m × 0.20 mm i.d., 0.33 μm capillary column (J&W Scientific). The overall level of HDC was converted to mol% conversion using detailed calibration plots. Quantitative analysis was based on relative peak area with acetone as solvent where analytical repeatability was better than ±1% and the detection limit corresponded to a feedstock conversion less than 0.1 mol%. HDC performance is quantified in terms of fractional dechlorination (X_{Cl})

$$X_{Cl} = \frac{[Cl_{org}]_{in} - [Cl_{org}]_{out}}{[Cl_{org}]_{in}} \quad (1)$$

where $[Cl_{org}]$ represents the molar rate ($mol_{Cl}\,h^{-1}$) of chlorine associated with the aromatic feed; *in* and *out* refer to the inlet and outlet reactor streams, respectively. It has been demonstrated previously [32,33] that HCl is the only inorganic product with no detectable Cl_2 production, *i.e.* $[Cl_{org}]_{in} - [Cl_{org}]_{out} = [HCl]_{out}$. A chlorine mass balance (in the form of HCl product) was performed by passing the effluent gas through an aqueous NaOH trap ($(3.5–8.0) \times 10^{-3}$ mol dm^{-3}, kept under constant agitation at ≥300 rpm) and monitoring continuously the pH change by means of a Hanna HI Programmable Printing pH Bench-Meter. The concentration of HCl generated was also measured by titrimetric analysis of the NaOH trap solution using a Metrohm (Model 728) Autotitrator ($AgNO_3$, combined Ag electrode); Cl mass balance was complete to better than ±6%. Reaction over the catalysts considered in this study did not generate any products resulting from aromatic ring hydrogenation, *i.e.* 100% selectivity in terms of chlorine removal, where a carbon balance was achieved to better than ±4%. Selectivity in terms of chlorobenzene (S_{CB}%) formation from 1,3-DCB is given by

$$S_{CB}\% = \frac{[\mathrm{CB}]_{out}}{[1,3\text{-DCB}]_{in} - [1,3\text{-DCB}]_{out}} \times 100 \quad (2)$$

Repeated reactions with different samples from the same batch of catalyst delivered raw data reproducibility that was better than ±5%. The goodness of the fits resulting from our kinetic modeling was assessed on the basis of the χ^2 (chi-square) test where

$$\chi^2 = \frac{\Sigma[r_i^{exp} - r_i^{calc}(x_i, y_i)]^2}{r_i^{calc}(x_i, y_i)} \quad (3)$$

and r_i^{exp} is the experimentally determined reaction rate, x_i the independent or lumped variables such as (P_{CB}/P_{H_2}), ($P_{CB}/P_{H_2}^{0.5}$) and (P_{CB}/P_{HCl}, P_{H_2}), and y_i is the lumped equilibrium and/or kinetic constants while the function $r_i^{calc}(x_i, y_i)$ represents the calculated reaction rate obtained from the kinetic model. Based on the degrees of freedom $N - P$ (number of data points − number of parameters) which equals 10 for CB and 16 for 1,3-DCB, the data fitting is considered acceptable at a significance level $\alpha = 0.05$, if $\chi^2 < 18$ and 26, respectively, according to the NIST chi-square distribution table [34]. The models were discriminated on the basis of the *F*-test [35] where % confidence was calculated from the ratio of residual sum of squares of the models and $N - P$.

3. Results and discussion

3.1. Catalyst characterization

The Pd loading and BET surface areas of the three silica supported Pd samples considered in this study are recorded in Table 1. Catalysts with Pd loading = 1.4, 5.4 and 8.3% (w/w) are denoted as Pd/SiO_2-I, Pd/SiO_2-II and Pd/SiO_2-III, respectively. The Pd dilute (Pd/SiO_2-I) sample exhibited a BET area close to that of the SiO_2 support (194 $m^2\,g^{-1}$), while the areas of the higher loaded samples were measurably lower, an effect that can be attributed to partial pore blocking by the Pd component. The temperature programmed reduction (TPR) profiles recorded for the three catalyst precursors are shown in Fig. 1. Each profile is dominated by a sharp

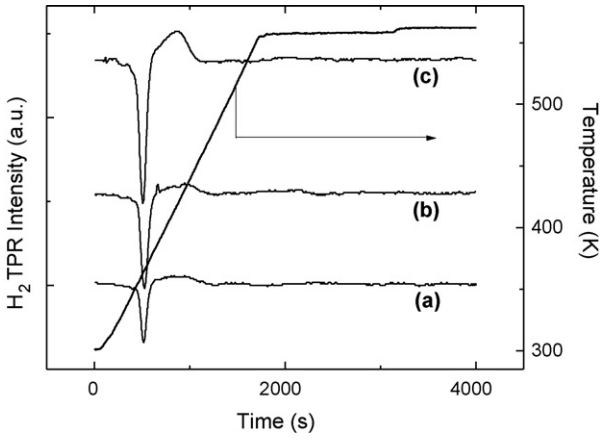

Fig. 1. TPR profiles generated for the direct reduction of (a) Pd/SiO_2-I, (b) Pd/SiO_2-II and (c) Pd/SiO_2-III.

Table 2
T_{max} values associated with TPR and H_2 TPD: entries given in bold font correspond to T_{max} for Pd hydride decomposition during TPR.

	TPR T_{max} (K)	TPD T_{max} (K)
Pd/SiO_2-I	**361**, 420	523, 873
Pd/SiO_2-II	**362**, 425	548, 873
Pd/SiO_2-III	**366**, 417	573, 873

negative peak representing H_2 release with an associated T_{max} in the range 361–366 K (see Table 2), which can be ascribed to the decomposition of β-palladium hydride that is formed at room temperature [36–39]. The absence of any H_2 consumption (during TPR) in advance of H_2 release/hydride decomposition presupposes the existence of a metallic phase prior to the commencement of the temperature ramp. Indeed, a room temperature reduction of PdO has been established elsewhere [8,36]. A hydrogen consumption peak was observed at 417–425 K (Fig. 1 and Table 2) that matches earlier reports in the literature [25,40] and can be attributed to the reduction of palladium species that interact more strongly with the support. Hydrogen consumption during the TPR of the Pd dilute Pd/SiO_2-I is negligible but the positive TPR signal is significant for the profile generated for Pd/SiO_2-III. Juszczyk et al. [41] in their TPR analysis of 1 and 10% (w/w) Pd/SiO_2 found that the former did not exhibit any H_2 consumption up to *ca.* 825 K while the higher metal loaded sample showed a strong peak at *ca.* 373 K. The H/Pd molar ratio associated with hydride decomposition (Table 1) is dependent on Pd loading with a lower ratio recorded for Pd/SiO_2-I. This response is supported by trends reported in the literature [42–44] suggesting higher H/Pd values with increasing Pd content and this has been linked to the presence of larger Pd particles. The hydride H/Pd ratio has been reported [44] to increase from 0.1 to 0.6 with an increase in the Pd loading from 0.3 to 2.8% (w/w); an upper value of 0.76 has been recorded for bulk Pd [45].

The representative TEM images provided in Fig. 2 serve to illustrate the nature of Pd metal dispersion; selected area electron diffraction (SAED) analysis confirmed the presence of Pd. The pseudo-spherical particle morphology is suggestive of relatively weak metal/support interaction. An increase in Pd loading resulted in a shift in Pd size range to deliver a greater mean Pd diameter (from 3.2 to 9.4 nm, see Table 1). The H_2 chemisorption values given in Table 1 reveal a greater total uptake for the higher Pd loading. We have avoided the assignment of Pd particle size or dispersion based on the chemisorption measurements as this presumes an exclusive H:Pd stoichiometry which is, at best, a convenient approximation. Our TEM analysis is based on a sufficiently high particle count (650) to ensure a valid measure of Pd size [46]. The TPD profiles (to 873 K) that followed H_2 chemisorption are recorded in Fig. 3; the characteristic T_{max} values are given in Table 2. Two desorption peaks characterize these profiles, *i.e.* a less intense ill-defined peak with an associated T_{max} in the range 523–573 K and an appreciably greater desorption that extends into the final isothermal hold. The amount of H_2 released at $T < 700$ K (lower temperature peak) matches that taken up in the chemisorption step (Table 1), which preceded TPD. The quantity of H_2 desorbed at higher temperatures was similar for all the samples and can be associated with spillover hydrogen. Spillover results from the migration of atomic hydrogen to the support after dissociation of molecular hydrogen on the metallic surface [47] and has been linked to desorption at $T > 600$ K, regardless of the nature of the metal and support [48,49]. Based on the entries given in Table 1, spillover hydrogen exceeded chemisorbed hydrogen by a factor of up to 35. This is significant in that spillover hydrogen has been proposed to contribute to catalytic HDC [30,50,51].

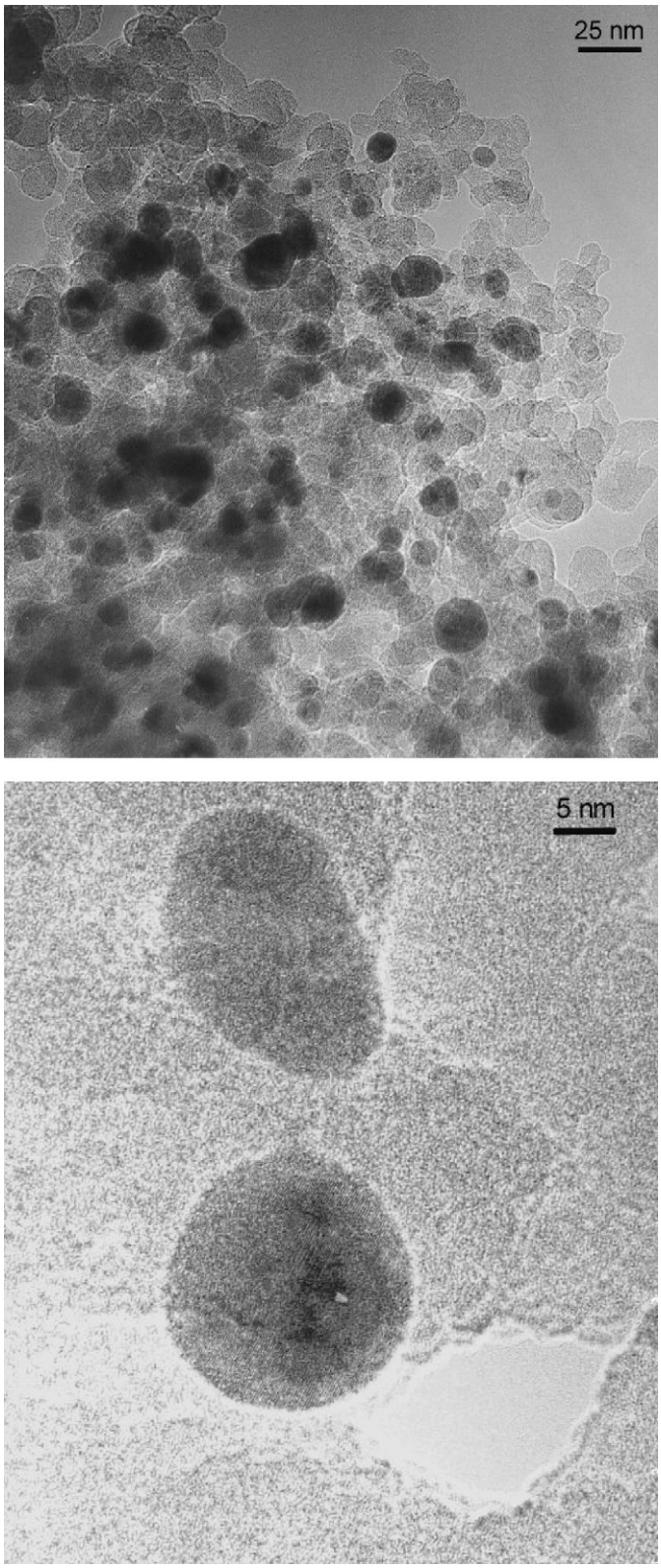

Fig. 2. Representative TEM images of Pd/SiO_2-III.

3.2. Catalyst performance

3.2.1. Evaluation of heat and mass transfer effects—establishment of kinetic regime

It is generally true that laboratory scale fixed-bed reactors approximate plug-flow behaviour [52]. In this study, the ratio of

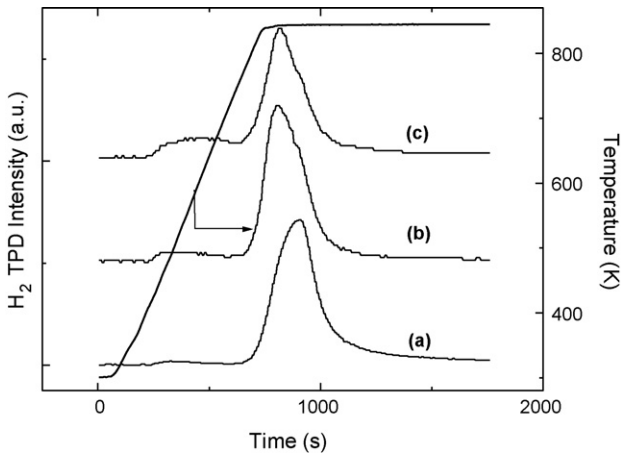

Fig. 3. H_2 TPD (to 873 K) associated with (a) Pd/SiO_2-I, (b) Pd/SiO_2-II and (c) Pd/SiO_2III.

reactor to catalyst particle diameter = 75 and the ratio of bed length to catalyst diameter = 140, exceeding the lower limits of 10 and 50, respectively, that are needed to satisfy the application of plug-flow conditions [53,54]. The existence of plug-flow ensures that by-pass or axial dispersion effects are reduced while maintaining a radially well mixed flow where transport gradients are minimized [17,54]. We adopted the fractional dechlorination (X_{Cl}, see Eq. (1)) obtained after 6 h on-stream as a measure of HDC performance. Under these conditions, HDC had reached a steady state that followed an initial induction period wherein X_{Cl} exhibited a temporal decline, as illustrated in Fig. 4. It should be noted that a similar approach has been applied by Coq et al. [27] in their kinetic study of CB HDC over supported Pd and Rh. We have used three established diagnostic criteria, *i.e.* variation of contact time (τ), linear velocity of the liquid feed at constant LHSV and particle size, to establish conditions wherein external and internal temperature/concentration gradients are minimized, taking Pd/SiO_2-I as a representative catalyst.

The effect of contact time on X_{Cl} is shown in Fig. 5(a) where it can be seen that HDC activity in the conversion of both CB and 1,3-DCB was largely insensitive to an increase in τ from 1.7 to 2.7 s, indicative of minimal external mass and/or heat transport contributions to the overall HDC. At $\tau < 1.7$ s, the significant decline in X_{Cl} is the result of transport constraints that serve to limit HDC. Taking the HDC of 1,3-DCB, a plot of selectivity (to CB) *vs.* fractional

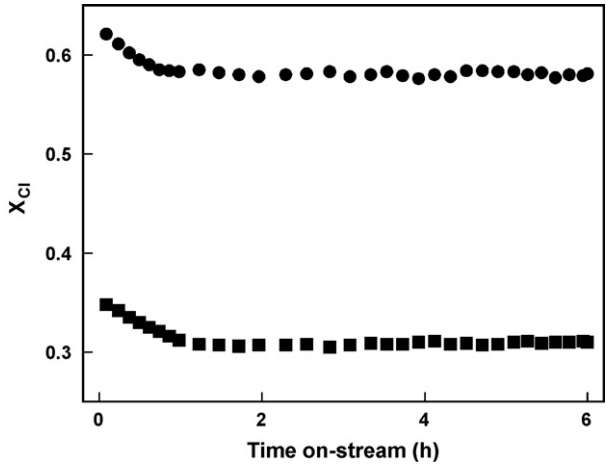

Fig. 4. Variation of fractional dechlorination (X_{Cl}) with time on-stream in the HDC of CB (■) and 1,3-DCB (●) over Pd/SiO_2-I: $P_{H_2} = 0.9$ atm; $T = 423$ K.

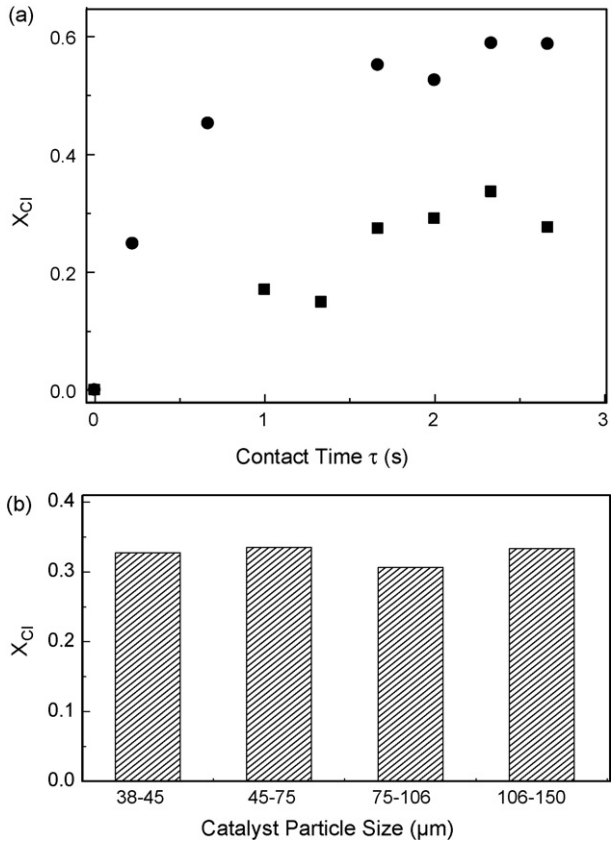

Fig. 5. (a) Variation of fractional dechlorination (X_{Cl}) with contact time (τ) in the HDC of CB (■) and 1,3-DCB (●) over Pd/SiO_2-I: $P_{H_2} = 0.9$ atm; $T = 423$ K. (b) Effect of catalyst particle size on the fractional dechlorination of CB over Pd/SiO_2-I: $T = 423$ K; $P_{H_2} = 0.9$ atm; $\tau = 2.3$ s.

DCB consumption, as shown in Fig. 6, is a useful means of probing changes in reaction pathway. HDC of DCB can proceed in a stepwise (to generate CB as a partially dechlorinated product) or a concerted fashion where the latter involves the concomitant scission of both Cl substituents to give benzene [7,55]. The activity/selectivity data (in Fig. 6) fall on a common trend line where $\tau > 0.2$ s but it is clear that there is no overlap with the data generated at $\tau = 0.2$ s. This is a significant finding, *i.e.* transport constraints result in a preferen-

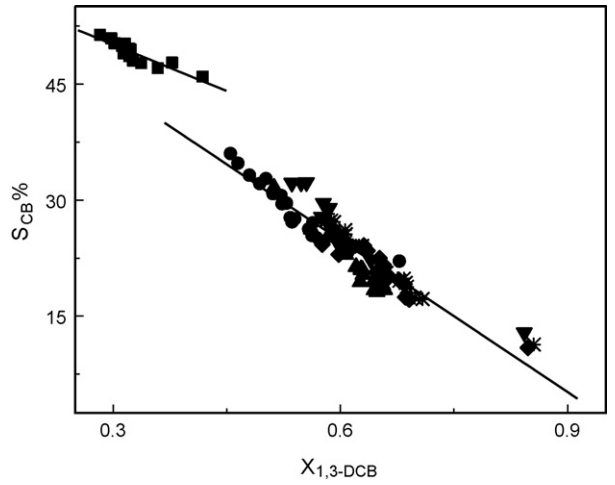

Fig. 6. Variation of selectivity to CB (S_{CB}) with fractional 1,3-DCB consumption ($X_{1,3\text{-}DCB}$) over Pd/SiO_2-I: $T = 423$ K; $P_{H_2} = 0.925$ atm; $\tau = 0.2$ s (■), 0.7 s (●), 1.7 s (▲), 2.0 s (▼), 2.3 s (♦) and 2.7 s (✱). *Note*: the linear fits represent trendlines.

Table 3
Effect of varying the linear liquid velocity of 1,3-DCB at a constant LHSV ($3\ h^{-1}$) on fractional dechlorination (X_{Cl}), fractional 1,3-DCB consumption ($X_{1,3\text{-}DCB}$) and HDC selectivity to CB (S_{CB}) after 6 h on-stream over Pd/SiO_2-I: $\tau = 2.3$ s; inlet hourly Cl/Pd mol ratio = 3.6×10^3; $T = 423$ K; inlet $P_{H_2} = 0.925$ atm.

Linear velocity ($cm^3\ h^{-1}$)	X_{Cl}	$X_{1,3\text{-}DCB}$	S_{CB} (%)
0.82	0.50	0.57	25
1.03	0.51	0.58	24
1.23	0.48	0.54	21
1.44	0.50	0.56	22

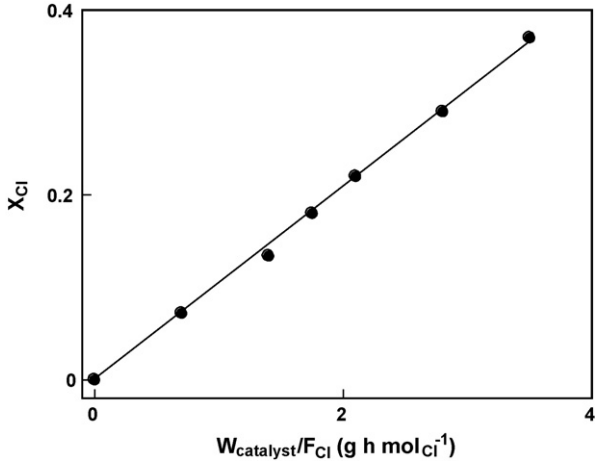

Fig. 7. Variation of fractional dechlorination (X_{Cl}) of 1,3-DCB with $W_{catalyst}/F_{Cl}$ over Pd/SiO_2-I: $T = 423$ K; $P_{H_2} = 0.46$ atm.

tial partial HDC. We are not aware of any report in the literature that demonstrates this response. Based on these results, the contact time for subsequent tests was set at 2.3 s. At this contact time, a variation of the 1,3-DCB linear velocity (0.19–0.33 μm s^{-1}) at a constant LHSV ($3\ h^{-1}$) was employed to further probe any variations in concentration gradients that can affect HDC activity/selectivity. The results are presented in Table 3 where it can be seen that HDC activity/selectivity was essentially insensitive to variations to the 1,3-DCB linear velocity, which suggests minimal interphase diffusion limitations. Particle size can impact on both interphase (temperature gradients as a result of the relatively higher thermal conductivity of the catalyst particles compared with the gas layer) and intraphase (intraparticle concentration gradients) transport. A series of HDC reactions conducted over a range of catalyst particle size (38–150 μm) revealed an X_{Cl} invariance (within experimental error, <2% mol/mol) as is shown in Fig. 5(b), indicating that external and/or internal transport effects do not contribute to HDC performance. Based on the foregoing results, gas phase CB/DCB HDC over Pd/SiO_2 operates under chemical/kinetic control where: $\tau = 2.3$ s; liquid feed rate = 0.014 $mol_{Cl}\ h^{-1}$; particle size = 45–75 μm. These process conditions were applied in the subsequent kinetic studies, which probe the effects of T (373–423 K) and P_{H_2} (0.046–0.925 atm) variations.

3.2.2. HDC kinetics

HDC kinetics under plug-flow conditions can be represented by the expression [56]

$$F_{Cl_{in}} \frac{dX_{Cl}}{dW} = r_{Cl} \tag{4}$$

where r_{Cl} is the total dechlorination rate ($mol_{Cl}\ h^{-1}\ g_{Pd}{}^{-1}$), W the catalyst weight (g) and $F_{Cl_{in}}$ is the inlet Cl_{org} flow rate ($mol_{Cl}\ h^{-1}$). The diagnostic tests described above established reaction conditions wherein concentration and temperature gradients in the catalyst bed were minimized and differential reactor conditions were operable. This was further validated by the linear response (passing through the origin) of X_{Cl} to variations in $W_{catalyst}/F_{Cl}$ as shown in Fig. 7, which confirms chemical control. Under differential reaction conditions, the following expression applies

$$r_{Cl} = F_{Cl_{in}} \frac{\Delta X_{Cl}}{W} \tag{5}$$

and where $F_{Cl_{in}}$ and W are constant, Eq. (5) reduces to

$$r_{Cl} = kX_{Cl} \tag{6}$$

where k is the pseudo-first order HDC rate constant. The dependence of r_{Cl} on H_2 partial pressure (P_{H_2}) at two selected temperatures (373 and 423 K) for the conversion of CB and 1,3-DCB is shown in Fig. 8(a) and (b), respectively, where an increase in HDC rate with P_{H_2} is evident. There is a dearth of published comprehensive HDC kinetic models that apply to supported metal catalysts. Lopez et al. [17] established pseudo-first order kinetics for the HDC of tetrachloroethylene, CB, DCB and dichloromethane over Pd/Al_2O_3 and demonstrated the applicability of Langmuir–Hinshelwood (L–H) single (competitive adsorption) and dual (non-competitive adsorption) site Models where the assumption of competitive adsorption of the chlororeactant and hydrogen on the same sites provided a better fit to the experimental results. Coq et al. [27] proposed a mechanism for the HDC of CB over alumina supported Pd and Rh catalysts involving competitive adsorption of CB and HCl for surface Pd-H sites generated as a result of dissociative H_2 adsorption and established reaction orders of 1, 0.5 and −1 for CB, H_2 and HCl, respectively. They further proposed HDC structure sensitivity where electron rich larger particles were intrinsically more active. Hagh and Allen [29] in their investigation of the HDC of 1,2-DCB over $NiMo/\gamma\text{-}Al_2O_3$ found that CB selectivity was dependent on CB desorption rate relative to surface HDC rate and proposed a competitive adsorption model involving dissociative hydrogen and associative CB uptake. The involvement of dissociative H_2 adsorption in HDC over supported Ni has been demonstrated elsewhere [30,42]. Taking an overview of the limited published kinetic analyses, the nature of the reactive chloroarene (associative or dissociative) remains open

Table 4
A comparison of the applicable Langmuir–Hinshelwood (L–H) models tested for CB and 1,3-DCB HDC with the corresponding site balance, rate expression, chi-square test (χ^2) results and % confidence with respect to Model B.

	Site balance	L–H Model, r_{Cl}=	χ^2		% confidence	
			CB	DCB	CB	DCB
Model **A**	$\theta_{ClA} + \theta_{H_2} = 1$	$\frac{k_{ClA}K_{H_2}K_{ClA}P_{H_2}P_{ClA}}{(K_{ClA}P_{ClA}+K_{H_2}P_{H_2})^2}$	1.5	4.8	**B** fits 86% better than **A**	**B** fits 91% better than **A**
Model **B**	$\theta_{ClA} + \theta_H = 1$	$\frac{k_{ClA}K_HK_{ClA}P_{H_2}P_{ClA}}{\left(K_{ClA}P_{ClA}+\sqrt{K_HP_{H_2}}\right)^3}$	0.8	2.3	–	–
Model **C**	$\theta_{ClA} + \theta_{HCl} = 1$, $\theta_z \gg \theta_H$	$\frac{k_{ClA}K_HK_{HCl}P_{H_2}P_{ClA}}{K_{HCl}P_{ClA}+P_{HCl}}$	1.6	3.9	**B** fits 86% better than **C**	**B** fits 99% better than **C**

θ_{HCl} represents HCl adsorption site; θ_z represents type II vacant sites for hydrogen adsorption.

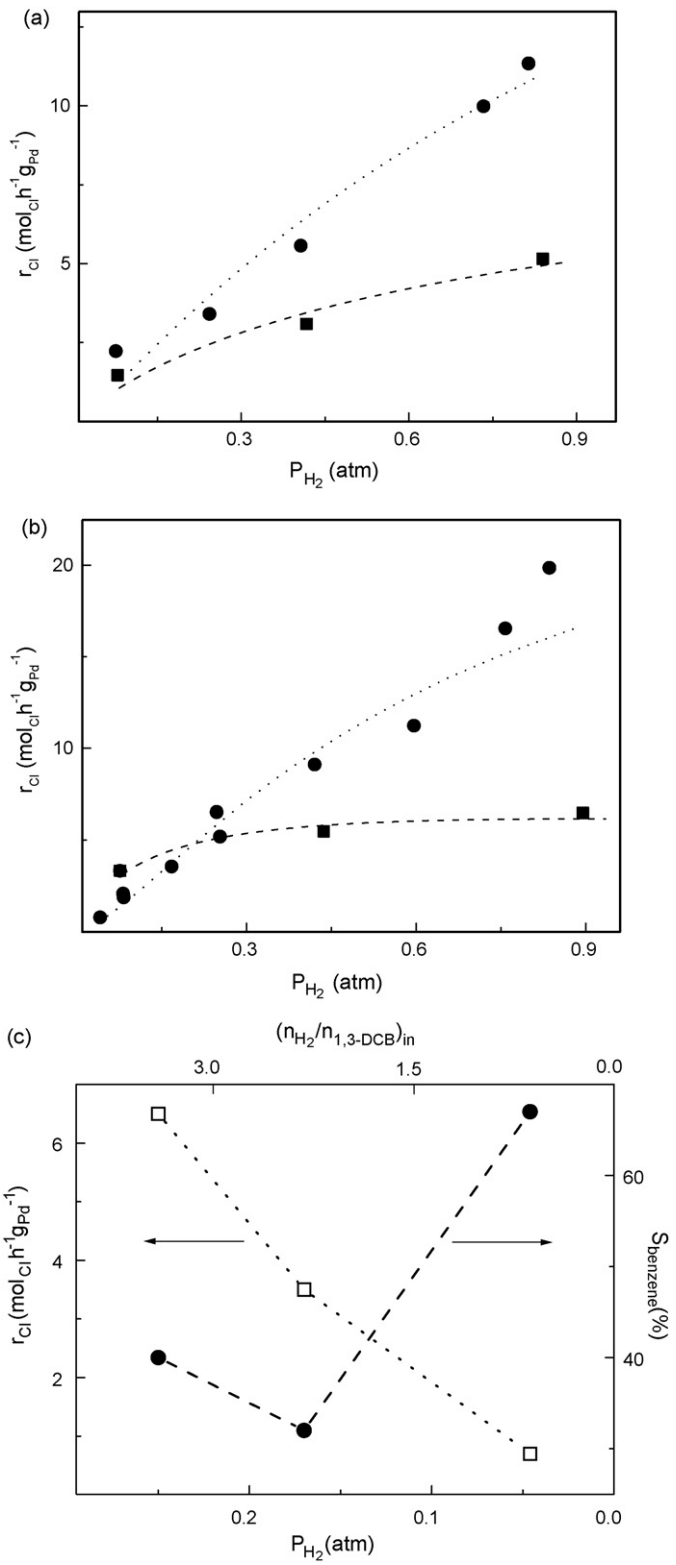

Fig. 8. (a) Variation of CB HDC rate (r_{Cl}) over Pd/SiO_2-I with P_{H_2} at T = 373 K (■, - - -) and 423 K (●, . . .). (b) Variation of 1,3-DCB HDC rate (r_{Cl}) over Pd/SiO_2-I with P_{H_2} at T = 373 K (■, - - -) and 423 K (●, . . .). *Note*: lines represent fit to the Model B from Eq. (11). (c) Variation of 1,3-DCB HDC rate (r_{Cl}, □) and $S_{benzene}$ (●) with P_{H_2} = 0.046–0.25 atm (inlet H_2/DCB mol/mol = 0.6–3.5) at 423 K.

to question as too is the applicability of a single or dual site mechanism.

As part of a preliminary kinetic treatment, the following Models were tested:

I Eley-Rideal mechanism where associatively adsorbed chloroarene reacts with H_2 gas [57];
II Dual site non-competitive associative adsorption of chloroarene (ClA) and dissociative adsorption of H_2 [58];
III Dual site non-competitive associative adsorption of both chloroarene and H_2;
IV Competitive dissociative adsorption of both ClA and H_2.

Each of these models generated negative equilibrium (for CB, DCB, H_2 or H) or lumped kinetic/equilibrium constants (for CB, DCB, H_2 or H) and can be discounted. The following Models provided acceptable fits to the experimental data as can be assessed from the entries in Table 4 wherein the applicable rate expressions are presented:

- Model A: competitive adsorption model based on the associative adsorption of H_2 and chloroaromatic (ClA = CB or 1,3-DCB) with no product inhibition;
- Model B: competitive adsorption model based on the associative adsorption of ClA and dissociative adsorption of H_2 with no product inhibition;
- Model C: non-competitive adsorption model based on associative adsorption of ClA (type I sites) and dissociative adsorption of H_2 (type II sites) where the HCl by-product adsorbed (on type I sites) was displaced by ClA reactant [42].

Model B provided a superior χ^2 response (see Section 2.2 for acceptable value for fit convergence) where the *F*-test delivered a confidence of 86–99% for Model B over Models A or C, *i.e.* an 86–99% confidence that Model B provides a better fit than Models A or C (see Table 4). Model B is based on a L–H type single site competitive adsorption model. The equilibration of the dissociative adsorption of hydrogen leads to the following relationship:

$$\theta_H = \sqrt{K_H P_{H_2}}\theta_V \tag{7}$$

where θ_H is the fractional surface coverage by dissociated *H*, K_H the associated adsorption equilibrium constant and θ_V is the fraction of vacant surface sites. An associative adsorption of the chloroarene can occur via Cl/Pd interactions [33] where

$$\theta_{ClA} = K_{ClA}P_{ClA}\theta_V \tag{8}$$

θ_{ClA} represents the fractional surface coverage by CB (or DCB) and K_{ClA} the associated equilibrium constant. Models A and B do not include any contribution due to HCl adsorption while in Model C, HCl is displaced by the chloroaromatic reactant. The rate determining surface reaction leads to the following equation for the overall reaction rate

$$r_{Cl} = k_{ClA}\theta_H^2\theta_{ClA} \tag{9}$$

where k_{ClA} is the surface rate constant and

$$\theta_{ClA} + \theta_H = 1 \tag{10}$$

at quasi-steady state. Solving Eqs. (7), (8) and (10) for θ_V and substitution into Eq. (9) yields the rate expression

$$r_{Cl} = \frac{k_{ClA}K_H K_{ClA}P_{H_2}P_{ClA}}{(K_{ClA}P_{ClA} + \sqrt{K_H P_{H_2}})^3} \tag{11}$$

Agreement of the Model B predicted r_{Cl} *vs.* P_{H_2} with the experimental values can be assessed in Fig. 8(a) and (b), where it can be seen that the Model captures the experimental response. It

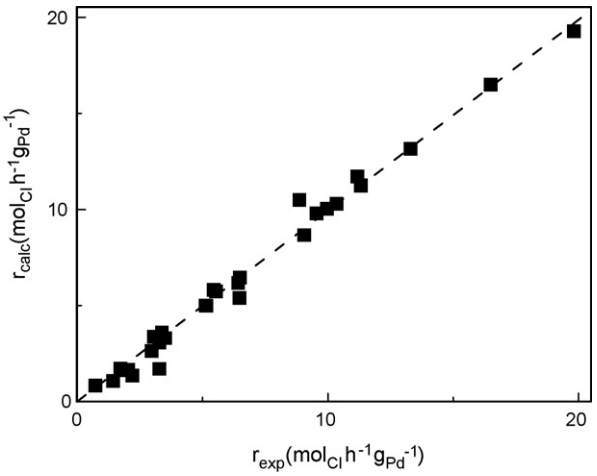

Fig. 9. Experimental (r_{exp}) and predicted (r_{calc} from Model B) CB and 1,3-DCB HDC rates associated with Pd/SiO_2-I: P_{H_2} = 0.046–0.925 atm; T = 373–423 K. r^2 = 0.99 and slope = 0.99 for the linear fit.

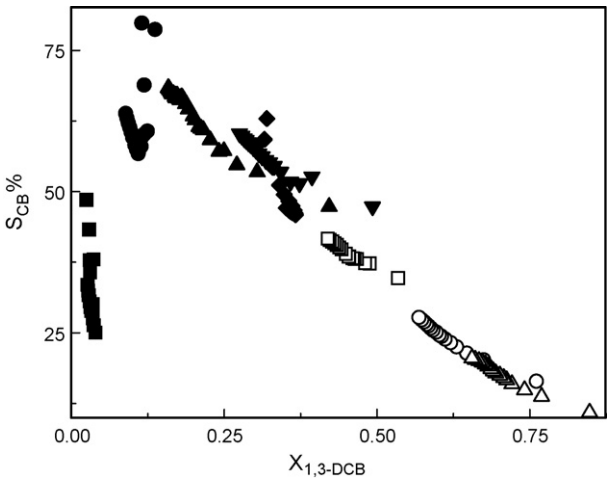

Fig. 10. The variation of HDC selectivity to CB (S_{CB}) as a function of fractional consumption of 1,3-DCB ($X_{1,3\text{-}DCB}$) over Pd/SiO_2-I where P_{H_2} (atm) = 0.046 (■), 0.092 (●), 0.19 (▲), 0.28 (▼), 0.46 (♦), 0.65 (□), 0.83 (○) and 0.925 (△): T = 423 K; inlet Cl/Pd mol ratio = 3.6×10^3 h^{-1}.

should be noted that the Model has been applied to experimental rate data that span over one order of magnitude from the lowest (1.4 $mol_{Cl}\,h^{-1}\,g_{Pd}{}^{-1}$) to the highest (19.8 $mol_{Cl}\,h^{-1}\,g_{Pd}{}^{-1}$) recorded rates. The parity plot shown in Fig. 9 serves to illustrate the level of agreement of the calculated with the experimental rates. In order to demonstrate that competitive adsorption is a feature of HDC, we have examined the HDC rate and selectivity responses for the conversion of 1,3-DCB at lower P_{H_2} (<0.3 atm) and the results (where T = 423 K) are shown in Fig. 8(c). A decrease in P_{H_2} resulted in a drop in the dechlorination rate (r_{Cl}) but there was a significant increase in the selectivity to benzene ($S_{benzene}$) at $P_{H_2} = 0.046$ atm, corresponding to an inlet molar ratio $n_{H_2}/n_{1,3\text{-DCB}} = 0.62$. This response suggests that at sub-stoichiometric inlet ratios, the displacement of CB (as an intermediate product) from a surface site due to competitive adsorption with hydrogen is not as prevalent and this results in a greater degree of complete HDC to benzene. In terms of the single site competitive model, an excess of H_2 relative to stoichiometric values elevates r_{Cl} as a result of an increase in surface hydrogen concentration. However, the excess H_2 also offers greater competition for surface sites resulting in a displacement of the adsorbed intermediate CB which, in turn, impacts on HDC selectivity. Hagh and Allen [29] have reported comparable rates of CB and benzene production from 1,2-DCB and concluded that the surface HDC and CB desorption rates are of the same magnitude.

3.2.3. *Influence of hydrogen partial pressure on HDC performance*

The relationship between fractional 1,3-DCB conversion ($X_{1,3\text{-}DCB}$) and HDC selectivity in terms of partial dechlorination (S_{CB}) resulting from variations in P_{H_2} (from 0.046 to 0.925 atm) at a representative temperature (423 K) is shown in Fig. 10. Where $P_{H_2} > 0.092$ atm (H_2/DCB > 1.25, H_2 in excess), selectivity to CB exhibits a consistent decline with increasing $X_{1,3\text{-}DCB}$ suggesting stepwise dechlorination as the predominant reaction pathway. Where $P_{H_2} \leq 0.092$ atm (H_2/DCB ≤ 1.25, stoichiometric to sub-stoichiometric ratios) an apparently anomalous trend arises, *i.e.* lower selectivities to CB at lower $X_{1,3\text{-}DCB}$. This may be reconciled in terms of the single site/competitive adsorption mechanism where at low inlet P_{H_2}, displacement/desorption of the partially dechlorinated CB through competition for surface sites is not as prevalent with the result that complete HDC is preferred. The same P_{H_2}/S_{CB} response was observed over the temperature range 373–423 K, *i.e.* enhanced benzene formation at $P_{H_2} \leq 0.092$ atm. With a view to assessing H_2 usage efficiency, the mol ratio of HDC products to H_2 in the exit stream is plotted as a function of inlet partial pressure for two representative temperatures in Fig. 11; HDC yields and selectivities are provided in Table 5. It is evident that operation at lower P_{H_2} translates into more effective hydrogen use in a single pass continuous operation. With respect to the issue of catalyst structure sensitivity, the specific

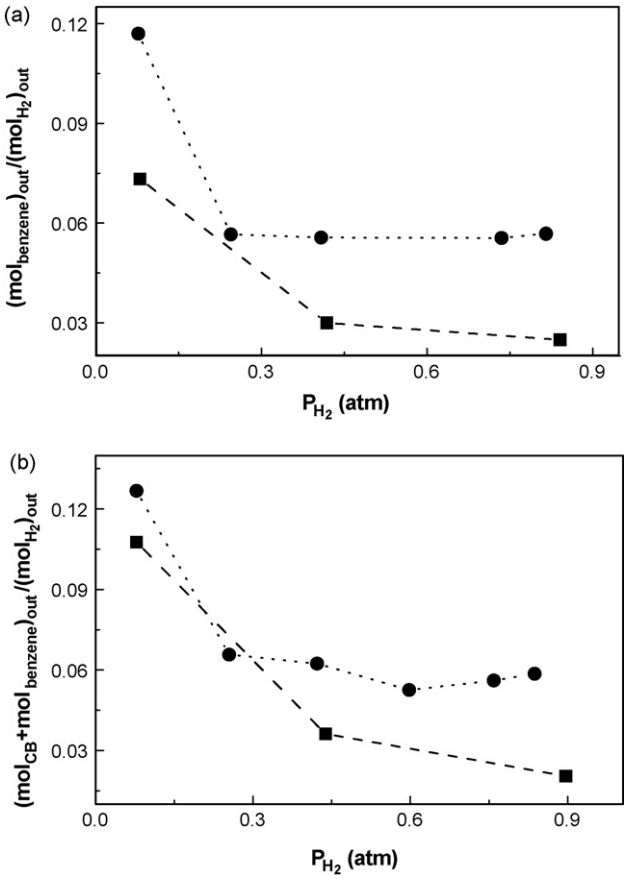

Fig. 11. Mol ratio of (a) benzene to H_2 ($(mol_{benzene})_{out}/(H_2)_{out}$) and (b) benzene + CB to H_2 ($(mol_{CB} + mol_{benzene})_{out}/(H_2)_{out}$) as a function of inlet P_{H_2} during the HDC of (a) CB and (b) 1,3-DCB over Pd/SiO_2-I: T = 373 K (■) and 423 K (●); inlet Cl/Pd mol ratio = 3.6×10^3 h^{-1}.

Table 5
Yield of benzene ($Y_{benzene}$) and chlorobenzene (Y_{CB}) from the HDC of CB and 1,3-DCB over Pd/SiO_2-I with varying P_{H_2}: $T = 373$ K; inlet hourly Cl/Pd mol ratio = 3.6×10^3.

P_{H_2} (atm)	HDC of CB	HDC of 1,3-DCB	
	$Y_{benzene}$ (%)	Y_{CB} (%)	$Y_{benzene}$ (%)
0.09	4.3	3.1	8.2 (74)[a]
0.45	9.1	10.1	11.1 (52)[a]
0.9	15.2	10.9	13.6 (55)[a]

[a] $S_{benzene}$ in parentheses.

Table 6
Specific HDC rates and associated selectivity (to CB) for the HDC of 1,3-DCB over the three Pd/SiO_2 catalysts: $P_{H_2} = 0.09$ atm; $T = 423$ K; inlet molar Cl/Pd = 3.6×10^3 h^{-1}.

Catalyst	r_{Cl} ($\times 10^{-3}$ mol_{Cl} h^{-1} $m_{Pd}{}^{-2}$)	S_{CB} (%)
Pd/SiO_2-I	12	27
Pd/SiO_2-II	27	26
Pd/SiO_2-III	37	29

rates and selectivities obtained at lower P_{H_2} (0.09 atm) over the three Pd/SiO_2 catalysts were measured and are recorded in Table 6. An increase in Pd loading was accompanied by higher specific rates where equivalent selectivities were obtained for the three systems. This response suggests higher intrinsic HDC activity associated with larger Pd particles (see Table 1) and is in line with observations reported elsewhere [41,59–63]. The implication in terms of enhancing HDC efficiency is to employ supported Pd catalysts bearing larger Pd particles (over the size range 3–9 nm). Hydrogen efficiency can be further improved by recycling unreacted hydrogen, a process modification that will be considered in future work.

4. Conclusion

The gas phase hydrodechlorination of CB and 1,3-DCB was performed in a single pass continuous flow fixed catalyst bed (Pd/SiO_2, 1.4–8.3%, w/w Pd) reactor over the T range 373–423 K. The H_2 partial pressure (P_{H_2}) was varied from 0.046 to 0.925 atm with the aim of (i) controlling HDC activity/selectivity and (ii) assessing efficiency in terms of H_2 usage. Temperature programmed reduction (TPR) generated supported Pd particles that exhibited a pseudo-spherical geometry with mean diameters in the range 3–9 nm and evidence of spillover hydrogen that exceeded chemisorbed hydrogen (by a factor of up to 35). A systematic analysis of the activity/selectivity response to variations in contact time, liquid linear velocity and catalyst particle size has established conditions necessary for chemical control, *i.e.* contact time (τ) = 2.33 s, liquid feed rate = 0.014 mol_{Cl} h^{-1} and catalyst particle size = 45–75 μm. Under conditions of transport limitations ($\tau < 1.7$ s), there is evidence that partial HDC is favoured. Where chemical control prevailed, a Langmuir–Hinshelwood type model is proposed to account for HDC performance with varying inlet H_2 partial pressure, involving competitive dissociative H_2 and associative chloroarene adsorption. The proposed model delivered an improved χ^2 response and 85–99% confidence of providing a better fit than models involving non-competitive adsorption and/or associative adsorption of both reactants. Benzene selectivity from 1,3-DCB increased where $P_{H_2} \leq 0.092$, a response that can be attributed to lesser competition of the chloroarene with hydrogen for the same surface sites with the result that CB is not displaced from the surface and complete HDC to benzene prevails. An increase in Pd loading and associated mean Pd particle size was accompanied by higher specific HDC rates, diagnostic of structure sensitivity. The viability of recycling the unreacted H_2 or operating multiple passes through the catalyst bed will be the subject of future work.

Acknowledgements

We acknowledge assistance with experimental measurements provided by Dr. A. Dozier, F. Cárdenas-Lizana and S. Gómez-Quero.

References

[1] USEPA, Locating and Estimating Air Emissions from Sources of Chlorobenzenes (Revised), Office of Air Quality Planning and Standards, Research Triangle Park, NC, 1994.
[2] J.K. Fawell, S. Hunt, Environmental Toxicology, Organic Pollutants, Ellis Horwood, Chichester, 1988.
[3] USEPA, Toxic Release Inventory, Public Data Release, Office of Pollution Prevention and Toxics, Washington, DC, 1991.
[4] USEPA, Chlorobenzene, OPPT Chemical Fact Sheets, Office of Pollution Prevention and Toxics, Washington, DC, 1995.
[5] S. Harrad, Persistent Organic Pollutants: Environmental Behaviour and Pathways for Human Exposure, Kluwer, Dordrecht, 2001.
[6] USEPA, The Inventory of Sources of Dioxin in the United States, EPA/600/P-98/00A2, Washington, DC, 1998.
[7] S. Jujjuri, E. Ding, S.G. Shore, M.A. Keane, Gas phase hydrodechlorination of chlorobenzenes over silica supported Pd and Pd/Yb, Appl. Organomet. Chem. 17 (2003) 493–498.
[8] S. Jujjuri, E. Ding, E.L. Hommel, S.G. Shore, M.A. Keane, Synthesis and characterization of novel silica supported Pd/Yb bimetallic catalysts: application in gas phase hydrodechlorination and hydrogenation, J. Catal. 237 (2006) 486–500.
[9] S. Jujjuri, E. Ding, S.G. Shore, M.A. Keane, A characterization of Ln–Pd/SiO_2 (Ln = La, Ce, Sm, Eu, Gd and Yb): correlation of surface chemistry with hydrogenolysis activity, J. Mol. Catal. A: Chem. 272 (2007) 96–107.
[10] S. Jujjuri, E. Ding, S.G. Shore, M.A. Keane, Novel one step preparation of silica supported Pd/Sr and Pd/Ba catalysts *via* an organometallic precursor: application in hydrodechlorination and hydrogenation, J. Mol. Catal. A: Chem. 294 (2008) 51–60.
[11] K.V. Murthy, P.M. Patterson, G. Jacobs, B.H. Davis, M.A. Keane, An exploration of activity loss during hydrodechlorination and hydrodebromination over Ni/SiO_2, J. Catal. 223 (2004) 74–85.
[12] G. Yuan, M.A. Keane, Liquid phase catalytic hydrodechlorination of 2, 4-dichlorophenol over carbon supported palladium: an evaluation of transport limitations, Chem. Eng. Sci. 58 (2002) 257–267.
[13] S. Gómez-Quero, F. Cárdenas-Lizana, M.A. Keane, Effect of metal dispersion on the liquid phase hydrodechlorination of 2,4-dichlorophenol over Pd/Al_2O_3, Ind. Eng. Chem. Res. 47 (2008) 6841–6853.
[14] F. Alonso, I.P. Beletskaya, M. Yus, Metal-mediated reductive hydrodehalogenation of organic halides, Chem. Rev. 102 (2002) 4009–4091.
[15] G. Centi, Supported palladium catalysts in environmental catalytic technologies for gaseous emissions, J. Mol. Catal. A: Chem. 173 (2001) 287–312.
[16] N. Lingaiah, P.S.S. Prasad, P.K. Rao, F.J. Berry, L.E. Smart, Structure and activity of microwave irradiated silica supported Pd–Fe bimetallic catalysts in the hydrodechlorination of chlorobenzene, Catal. Commun. 3 (2002) 391–397.
[17] E. Lopez, S. Ordóñez, H. Sastre, F.V. Diez, Kinetic study of the gas-phase hydrogenation of aromatic and aliphatic organochlorinated compounds using a Pd/Al_2O_3 catalyst, J. Hazard. Mater. B 97 (2003) 281–294.
[18] S. Ordóñez, H. Sastre, F.V. Díez, Hydrodechlorination of tetrachloroethene over Pd/Al_2O_3: influence of process conditions on catalyst performance and stability, Appl. Catal. B: Environ. 40 (2003) 119–130.
[19] F.J. Urbano, J.M. Marinas, Hydrogenolysis of organohalogen compounds over palladium supported catalysts, J. Mol. Catal. A: Chem. 173 (2001) 329–345.
[20] A.Yu. Stakheev, L.M. Kustov, Effects of the support on the morphology and electronic properties of supported metal clusters: modern concepts and progress in 1990s, Appl. Catal. A: Gen. 188 (1999) 3–35.
[21] S.B. Halligudi, B.M. Devassay, A. Ghosh, V. Ravikumar, Kinetic study of vapor phase hydrodechlorination of halons by Pd supported catalysts, J. Mol. Catal. A: Chem. 184 (2002) 175–181.
[22] A. Gampine, D.P. Eyman, Catalytic hydrodechlorination of chlorocarbons. 2. Ternary oxide supports for catalytic conversions of 1,2-dichlorobenzene, J. Catal. 179 (1998) 315–325.
[23] R. Gopinath, K.N. Rao, P.S.S. Prasad, S.S. Madhavendra, S. Narayanan, G. Vivekanandan, Hydrodechlorination of chlorobenzene on Nb_2O_5-supported Pd catalysts: influence of microwave irradiation during preparation on the stability of the catalyst, J. Mol. Catal. A: Chem. 181 (2002) 215–220.
[24] M.A. Keane, Treating difficult and toxic chlorinated waste, Environ. Bus. Mag. 70 (2001) 12–14.
[25] M.A. Keane, Hydrodehalogenation over supported Ni and Pd: a comparative study, Appl. Catal. A: Gen. 271 (2004) 109–118.
[26] P. Bodnariuk, B. Coq, G. Ferrat, F. Figueras, Carbon-chlorine hydrogenolysis over PdRh and PdSn bimetallic catalysts, J. Catal. 116 (1989) 459–466.
[27] B. Coq, G. Ferrat, F. Figueras, Conversion of chlorobenzene over palladium and rhodium catalysts of widely varying dispersion, J. Catal. 101 (1986) 434–445.
[28] R. Gopinath, N. Lingaiah, B. Sreedhar, I. Suryanarayana, P.S.S. Prasad, A. Obuchi, Highly stable Pd/CeO_2 catalyst for hydrodechlorination of chlorobenzene, Appl. Catal. B: Environ. 46 (2003) 587–594.

[29] B.F. Hagh, D.T. Allen, Catalytic processing of chlorinated benzenes, AIChE J. 36 (1990) 773–778.
[30] M.A. Keane, D.Yu. Murzin, A kinetic treatment of the gas phase hydrodechlorination of chlorobenzene over nickel/silica: beyond conventional kinetics, Chem. Eng. Sci. 56 (2001) 3185–3195.
[31] K.V. Murthy, P.M. Patterson, M.A. Keane, C-X bond reactivity in the catalytic hydrodehalogenation of haloarenes over unsupported and silica supported Ni, J. Mol. Catal. A: Chem. 225 (2005) 149–160.
[32] C. Menini, C. Park, E.-J. Shin, G. Tavoularis, M.A. Keane, Catalytic hydrodechlorination as a detoxification methodology, Catal. Today 62 (2000) 355–366.
[33] G. Tavoularis, M.A. Keane, Gas phase catalytic hydrodechlorination of chlorobenzene over nickel/silica, J. Chem. Technol. Biotechnol. 74 (1999) 60–70.
[34] NIST/SEMATECH, e-Handbook of Statistical Methods, 2005.
[35] R.I. Masel, Chemical Kinetics and Catalysis, John Wiley & Sons, New York, 2001.
[36] C. Amorim, G. Yuan, P.M. Patterson, M.A. Keane, Catalytic hydrodechlorination over Pd supported on amorphous and structured carbon, J. Catal. 234 (2005) 268–281.
[37] F.B. Noronha, M. Schmal, B. Moraweck, P. Delichère, M. Brun, F. Villain, R. Fréty, Characterization of niobia-supported palladium–cobalt catalysts, J. Phys. Chem. B 104 (2000) 5478–5485.
[38] P.A. Weyrich, H. Treviño, W.F. Hölderich, W.M.H. Sachtler, Characterization of Ce promoted, zeolite supported Pd catalysts, Appl. Catal. A: Gen. 163 (1997) 31–44.
[39] C. Yang, J. Ren, Y. Sun, Role of La_2O_3 in Pd-supported catalysts for methanol decomposition, Catal. Lett. 84 (2002) 123–129.
[40] S. Karski, I. Witońska, I. Rogowski, J. Gołuchowska, Interaction between Pd and Ag on the surface of silica, J. Mol. Catal. A: Chem. 240 (2005) 155–163.
[41] W. Juszczyk, Z. Karpiński, D. Łomot, J. Pielaszek, Z. Paál, A.Yu. Stakheev, The structure and activity of silica-supported palladium cobalt alloys. 1. Alloy homogeneity, surface composition and activity for neopentane conversion, J. Catal. 142 (1993) 617–629.
[42] N.K. Nag, A study on the formation of palladium hydride in a carbon-supported palladium catalyst, J. Phys. Chem. B 105 (2001) 5945–5949.
[43] S.C. Shekar, K.S.R. Rao, E.S. Demessie, Characterization of palladium supported on gamma-Al_2O_3 catalysts in hydrodechlorination of CCl_2F_2, Appl. Catal. A: Gen. 294 (2005) 235–243.
[44] M. Skotak, Z. Karpinski, W. Juszczyk, J. Pielaszek, L. Kepinski, D.V. Kazachkin, V.I. Kovalchuk, J.L. d'Itri, Characterization and catalytic activity of differently pretreated Pd/Al_2O_3 catalysts: the role of acid sites and of palladium–alumina interactions, J. Catal. 227 (2004) 11–25.
[45] N. Nishimiya, T. Kishi, T. Mizushima, A. Matsumoto, K. Tsutsumi, Hyperstoichiometric hydrogen occlusion by palladium nanoparticles included in NaY zeolite, J. Alloys Compd. 319 (2001) 312–321.
[46] C. Amorim, M.A. Keane, Palladium supported on structured and non-structured carbon: a consideration of Pd particle size and the nature of reactive hydrogen, J. Colloid. Interf. Sci. 332 (2008) 196–208.
[47] W.C. Conner Jr., J.L. Falconer, Spillover in heterogeneous catalysis, Chem. Rev. 95 (1995) 759–788.
[48] F. Benseradj, F. Sadi, M. Chater, Hydrogen spillover studies on diluted Rh/Al_2O_3 catalyst, Appl. Catal. A: Gen. 228 (2002) 135–144.
[49] E.-J. Shin, A. Spiller, G. Tavoularis, M.A. Keane, Chlorine–nickel interactions in gas phase catalytic hydrodechlorination: catalyst deactivation and the nature of reactive hydrogen, Phys. Chem. Chem. Phys. 1 (1999) 3173–3181.
[50] Y. Hashimoto, A. Ayame, Low-temperature hydrodechlorination of chlorobenzenes on platinum-supported alumina catalysts, Appl. Catal. A: Gen. 250 (2003) 247–254.
[51] L.M. Gomez-Sainero, A. Cortes, X.L. Seoane, A. Arcoya, Hydrodechlorination of carbon tetrachloride to chloroform in the liquid phase with metal-supported catalysts. Effect of the catalyst components, Ind. Eng. Chem. Res. 39 (2000) 2849–2854.
[52] O. Levenspeil, Chemical Reaction Engineering, John Wiley, New York, 1972.
[53] G. Froment, K.B. Bischoff, Chemical Reactor Analysis and Design, John Wiley, New York, 1990.
[54] C. Perego, S. Peratello, Experimental methods in chemical kinetics, Catal. Today 52 (1999) 133–145.
[55] B.F. Hagh, D.T. Allen, Catalytic hydroprocessing of chlorobenzene and 1,2-dichlorobenzene, Chem. Eng. Sci. 45 (1990) 2695–2701.
[56] H.H. Lee, Heterogeneous Reactor Design, Butterworth Publishers, Boston, 1985.
[57] P. Dini, J.C.J. Bart, N. Giordano, Properties of polyamide-based catalysts 1. Hydrodehalogenation of chlorobenzene, J. Chem. Soc., Perkin Trans. 214 (1975) 1479–1482.
[58] C. Park, C. Menini, J.L. Valverde, M.A. Keane, Carbon–chlorine and carbon–bromine bond cleavage in the catalytic hydrodehalogenation of halogenated aromatics, J. Catal. 211 (2002) 451–463.
[59] T. Janiak, J. Błazejowski, Hydrogenolysis of chlorobenzene, dichlorobenzenes and chlorotoluenes by in situ generated and gaseous hydrogen in alkaline media and the presence of Pd/C catalyst, Chemosphere 48 (2002) 1097–1102.
[60] M.A Aramendia, V. Borau, I.M. Garcia, C. Jimenez, F. Lafont, A. Marinas, J.M. Marinas, F.J. Urbano, Influence of the reaction conditions and catalytic properties on the liquid-phase hydrodechlorination of chlorobenzene over palladium-supported catalysts: activity and deactivation, J. Catal. 187 (1999) 392–399.
[61] M.A. Keane, C. Park, C. Menini, Structure sensitivity in the hydrodechlorination of chlorobenzene over supported nickel, Catal. Lett. 88 (2003) 89–94.
[62] G. Pina, C. Louis, M.A. Keane, Nickel particle size effects in catalytic hydrogenation and hydrodechlorination: phenolic transformations over nickel/silica, Phys. Chem. Chem. Phys. 5 (2003) 1924–1931.
[63] W. Juszczyk, A. Malinowski, Z. Karpiński, Hydrodechlorination of CCl_2F_2 (CFC-12) over gamma-alumina supported palladium catalysts, Appl. Catal. A: Gen. 166 (1998) 311–319.